

# Estimating Evapotranspiration Over Native Wet Montane Cloud Forests in Hawai'i and Evaluating the Impact of Climate Change on it

## Basic Information

<b>Title:</b>	Estimating Evapotranspiration Over Native Wet Montane Cloud Forests in Hawai'i and Evaluating the Impact of Climate Change on it
<b>Project Number:</b>	2014HI431B
<b>Start Date:</b>	3/1/2014
<b>End Date:</b>	2/28/2016
<b>Funding Source:</b>	104B
<b>Congressional District:</b>	1
<b>Research Category:</b>	Climate and Hydrologic Processes
<b>Focus Category:</b>	Hydrology, Models, Water Quantity
<b>Descriptors:</b>	None
<b>Principal Investigators:</b>	Sayed Bateni

## Publications

1. Xu, T., S. Bateni, S. Liang, D. Entekhabi, and K. Mao, 2014, "Estimation of surface turbulent heat fluxes via variational assimilation of sequences of land surface temperatures from Geostationary operational environmental satellites," *Journal of Geophysical Research: Atmospheres*, 119(18), 10780-10798.
2. Xu, T., S. Bateni, and S. Liang, "Estimating Turbulent fluxes with a weak-constraint data assimilation scheme: A case study (HiWATER-MUSOEXE)," 2015, *IEEE Geoscience and Remote Sensing Letters*, 12(1), 68-72.

## Problem and Research Objectives

Sensible and latent heat fluxes are the key variables in energy and water vapor exchange between the land surface and the atmosphere. Latent heat flux is the coupling link between the surface water, energy, and carbon exchanges with the atmosphere. Several techniques (e.g., lysimeters, eddy covariance systems, Bowen ratio methods, and large-aperture scintillometers) have been used to measure surface heat fluxes (Liu et al., 2011, 2013). However, in situ measurements of heat fluxes are costly and are therefore distributed sparsely, and cover only limited time periods. Consequently, a number of models have been developed to estimate surface heat fluxes from remotely sensed land surface temperature (LST) observations.

LST lies at the heart of the surface energy balance (SEB) equation. All components of the SEB equation (i.e., sensible, latent, and ground heat fluxes as well as net radiation) are related to LST. Recently, Bateni and Entekhabi (2012a) showed that LST observations contain implicit information on the partitioning of available energy among the SEB components. LST observations have been utilized in three main groups of studies to estimate surface heat fluxes. The first group of studies is diagnostic. These studies use LST to solve the SEB equation and retrieve surface energy fluxes (Norman et al., 1995; Anderson et al., 1997; Bastiaanssen et al., 1998a, 1998b; Su, 2002; Liu et al., 2007; Jia et al., 2009; Ma et al., 2012). The ground heat flux is usually taken as an empirical fraction of the net radiation. Additionally, surface heat fluxes can be retrieved only for instances in which remotely sensed LSTs are available. The second group is known as triangle approaches. These studies attempt to estimate the surface evaporation using empirical relationships between LST and vegetation indices such as the normalized difference vegetation index and leaf area index (LAI) (Jiang and Islam, 2001, 2003; Nishida et al., 2003; Wang et al., 2006; Tang et al., 2010; Sun et al., 2013). These methods need to define the dry and wet edges of the triangle space, which is site specific.

The third group of studies estimates the surface heat fluxes by assimilating sequences of LST measurements within a variational data assimilation (VDA) framework using the parsimonious force-restore equation as a constraint (Castelli et al., 1999; Boni et al., 2001; Caparrini et al., 2003, 2004a, 2004b; Crow and Kustas, 2005; Qin et al., 2007; Sini et al., 2008). In contrast to the diagnostic and triangle approaches, this group of methods does not require any empirical or site-specific relationships and can provide temporally continuous surface heat flux estimates from discrete spaceborne LST observations.

The VDA utilizes combined-source (CS) and dual-source (DS) schemes to simulate interaction between the land surface and the overlying air and to retrieve surface heat fluxes. The CS scheme does not distinguish the difference between soil and canopy temperatures and treats LST as the effective temperature of a mixed soil-vegetation medium. In contrast, the DS scheme accounts for the difference between soil and canopy temperatures and considers the interactions of the soil and canopy with the overlying atmosphere separately.

Bateni and Liang (2012) and Bateni et al. (2013a, 2013b) significantly advanced the CS and DS VDA approaches by using the full heat diffusion equation as a physical constraint instead of the simple force-restore equation. However, the CS and DS VDA approaches by Bateni and Liang (2012) and Bateni et al. (2013a, 2013b) have been tested so far at only two humid sites with grassland vegetation cover (i.e., the First International Experiment and the Southern Great Plains sites). In this study, the performance of the recently augmented CS and DS VDA frameworks is assessed in detail using surface heat fluxes collected at six FluxNet sites with different vegetation covers (grassland, cropland, and forest) and climate conditions. These

sites are chosen because they sample different climatic and vegetative conditions in an effort to evaluate the robustness of the VDA schemes in various hydrological environments.

Sequences of daytime LST observations have various diurnal amplitudes depending on the available energy and the relative efficiency of SEB components (Bateni and Entekhabi, 2012a). Hence, an accurate characterization of the LST diurnal cycle is of vital importance for the reliable performance of the VDA methods. In this study, LST data from Geostationary Operational Environmental Satellites (GOES) are assimilated in the CS and DS VDA schemes to estimate surface heat fluxes. GOES can accurately characterize the LST diurnal cycle by providing LST data every 30 min and thus can significantly advance the robustness of the VDA framework. GOES LST can be accurately retrieved (Sun et al., 2004) and proved to be a significant data set for improving turbulent flux estimates of the land surface model (Xu et al., 2011).

## Methodology

### Heat Diffusion Equation

The soil temperature at depth  $z$  and time  $t$ ,  $T(z,t)$ , is given by the heat diffusion equation, which is given by

$$C \frac{\partial T(z,t)}{\partial t} = P \frac{\partial^2 T(z,t)}{\partial z^2} \quad (1)$$

where  $C$  and  $P$  are, respectively, the soil volumetric heat capacity ( $\text{J m}^{-3} \text{K}^{-1}$ ) and thermal conductivity ( $\text{Wm}^{-1}\text{K}^{-1}$ ). For simplicity,  $T(z = 0,t)$  is indicated by  $T(t)$ .

The boundary conditions at the top and bottom of the soil column are required to solve the heat diffusion equation. The boundary condition at the top of the soil column,  $T(z = 0,t)$ , is retrieved from the surface boundary forcing equation  $P dT(z = 0,t)/dz = G(t)$  (where  $G(t)$  is the ground heat flux at time  $t$ ) (Bateni et al., 2013a). At the bottom boundary, a Neumann boundary condition is implemented as

$$\frac{\partial T(l,t)}{\partial z} = 0 \quad (2)$$

where  $l$  is the depth of the bottom boundary condition, which is set to 0.5 m (Hu and Islam, 1995; Bateni and Liang, 2012; Bateni et al., 2013a). The heat diffusion equation is solved using an implicit finite difference scheme. The detailed information on discretization of the heat diffusion equation and its numerical implementation can be found in Bateni et al. (2012).

### Surface Energy Balance (SEB)

The CS SEB scheme considers the soil and vegetation as a single source and follows Bateni et al. (2013a). For the CS approach, the land surface energy balance equation can be written as

$$G = R_N - H - LE \quad (3)$$

where  $G$  is the ground heat flux ( $\text{Wm}^{-2}$ ),  $H$  and  $LE$  are the sensible and latent heat fluxes ( $\text{Wm}^{-2}$ ), and  $R_N$  is the net radiation ( $\text{Wm}^{-2}$ ) that is obtained according to Bateni et al. (2013a).

The sensible heat flux can be obtained with the LST ( $T$ ) generated by the heat diffusion equation as follows:

$$H = \rho c_p C_H U(T - T_A) \quad (4)$$

where  $\rho$  is the air density ( $\text{kg m}^{-3}$ ),  $c_p$  is the heat capacity of air ( $1012 \text{ J kg}^{-1} \text{ K}^{-1}$ ),  $U$  and  $T_A$  are, respectively, the wind speed ( $\text{m s}^{-1}$ ) and air temperature (K) at a reference height, and  $C_H$  is the bulk heat transfer coefficient (-). The bulk heat transfer coefficient ( $C_H$ ) can be written as the product of the neutral bulk heat transfer coefficient ( $C_{HN}$ ) and a correction function for atmospheric stability,  $f(Ri)$  (i.e.,  $C_H = C_{HN} f(Ri)$ , where  $Ri$  is the Richardson number).  $C_{HN}$  can be related to roughness length scales for heat and momentum (Liu et al., 2007; Zhang et al., 2010), which is mainly a function of vegetation phenology and is assumed to vary on a monthly temporal scale (McNaughton and Van den Hurk, 1995; Jensen and Hummelshøj, 1995; Qualls and Brutsaert, 1996; Crow and Kustas, 2005; Bateni et al., 2013b). It scales the sum of turbulent heat fluxes ( $H + LE$ ) and constitutes the first unknown parameter of the CS scheme. Following Crow and Kustas (2005), Sini et al. (2008), Bateni and Liang (2012), and Bateni and Entekhabi (2012b), the atmospheric correction function ( $f$ ) proposed by Caparrini et al. (2003) is used herein.

The second unknown of the CS scheme is evaporative fraction ( $EF$ ), which scales partitioning between the turbulent heat fluxes and is given by

$$EF = \frac{LE}{H+LE} \quad (5)$$

The DS SEB scheme developed by Bateni and Liang (2012) is used in this study. The DS can model interaction within the soil-canopy-atmosphere system (Kustas et al., 1996; Bateni and Liang, 2012). In the DS SEB model, the net radiation absorbed by the canopy ( $R_{NC}$ ) is partitioned between the sensible ( $H_C$ ) and latent ( $LE_C$ ) heat fluxes for the canopy ( $R_{NC} = H_C + LE_C$ , the subscript “C” refers to the vegetation canopy). The ground heat flux ( $G$ ) can be calculated as the residual of the surface energy balance for soil (Bateni and Liang, 2012).

The sensible heat fluxes for the canopy ( $H_C$ ) and soil ( $H_S$ ) can be estimated via (Bateni and Liang, 2012)

$$H_C = \rho c_p C_{HC} U_W(T_C - T_W) \quad (6a)$$

$$H_S = \rho c_p C_{HS} U_W(T_S - T_W) \quad (6b)$$

where  $U_W$  and  $T_W$  are, respectively, the wind speed and air temperature at a reference height within the canopy,  $T_C$  and  $T_S$  are the canopy and soil temperatures, and  $C_{HC}$  and  $C_{HS}$  are the bulk heat transfer coefficients from leaves and soil to air within the canopy (-).  $T_S$  is estimated with the heat diffusion equation (equation (1)). Equations for the estimation of  $T_C$  and  $T_W$  can be found in Bateni and Liang (2012).  $C_{HC}$  and  $C_{HS}$  are related to  $C_{HN}$  to decrease the number of unknown parameters of the DS scheme. For detailed information, the reader is referred to Bateni and Liang (2012) and Bateni et al. (2013b).

The total sensible heat flux ( $H$ ) can be estimated via

$$H = \rho c_p C_H U (T_W - T_A) \quad (7)$$

Similar to the CS SEB scheme,  $C_H$  is related to  $C_{HN}$  via  $C_H = C_{HN} f(Ri)$ . The total sensible heat flux ( $H$ ) is also given by the weighted average of sensible heat flux from the canopy and soil:

$$H = f_c H_c + (1 - f_c) H_s \quad (8)$$

where  $f_c$  is the vegetation cover fraction. The evaporative fractions for the soil and canopy ( $EF_s$  and  $EF_c$ ) are the other unknown parameters of the DS scheme and are given by

$$EF_c = \frac{LE_c}{H_c + LE_c} \quad (9a)$$

$$EF_s = \frac{LE_s}{H_s + LE_s} \quad (9b)$$

$C_{HN}$ ,  $EF_s$  and  $EF_c$  are the three unknown parameters of the DS SEB scheme that are estimated via a VDA framework.

In the DS SEB scheme, the effective LST is calculated through a composite of the soil and canopy temperatures are follows:

$$T = [f_c T_c^4 + (1 - f_c) T_s^4]^{0.25} \quad (10)$$

### Adjoint State Formulation

As mentioned in the previous section,  $C_{HN}$  and  $EF$  constitute the unknown parameters of the CS SEB scheme that should be estimated by the VDA approach. In the DS SEB model, three unknown parameters (i.e.,  $C_{HN}$ ,  $EF_c$  and  $EF_s$ ) must be estimated.  $C_{HN}$  varies on a monthly time scale (i.e., the scale of vegetation phenology) and thus one  $C_{HN}$  value is retrieved in each monthly modeling period (Caparrini et al., 2003, 2004a, b; Crow and Kustas, 2005; Bateni and Liang, 2012; Bateni and Entekhabi, 2012b; Bateni et al., 2013a, b).  $EF$  is self-preserved during daytime hours (i.e., 09:00–16:00 LT), but it can vary from day to day (Gentine et al., 2007).

A cost function ( $J$ ) is defined to retrieve the unknown parameters of the CS scheme (i.e.,  $C_{HN}$  and  $EF$ ) by minimizing the difference between the LST observations (from GOES) and estimates (from the heat diffusion equation). The cost function for the CS model can be written as

$$\begin{aligned} J(T, R, EF, \lambda) = & \sum_{i=1}^N \int_{t_0}^{t_1} [T_{OBS,i}(t) - T_i(t)]^T K_T^{-1} [T_{OBS,i}(t) - T_i(t)] dt \\ & + (R - R')^T K_R^{-1} (R - R') + \sum_{i=1}^N (EF_i - EF_i')^T K_{EF}^{-1} (EF_i - EF_i') \\ & + 2 \sum_{i=1}^N \int_{t_0}^{t_1} \int_0^J \lambda_i(z, t) \left[ \frac{\partial T_i(z, t)}{\partial t} - D \frac{\partial^2 T_i(z, t)}{\partial z^2} \right] dz dt \end{aligned} \quad (11)$$

The first term on the right-hand side of Eq. (11) measures the difference between the GOES-measured LST ( $T_{OBS}$ ) and the predicted LST ( $T$ ).  $C_{HN}$  is transformed to  $R$  via  $C_{HN} = \exp(R)$  to make it strictly positive and meaningful. The second and third terms measure the difference between the parameter estimates ( $R$  and  $EF$ ) and their prior values ( $R'$  and  $EF'$ ). As previously mentioned,  $C_{HN}$  is hypothesized to be constant over the entire monthly assimilation period ( $N = 30$  days), and  $EF$  is postulated to be invariant over each day during the assimilation window (i.e., from  $t_0 = 9:00$  to  $t_1 = 16:00$  LT). The last term is the heat diffusion equation, which is adjoined to the model (as a physical constraint) via the Lagrange multiplier,  $\lambda$ .  $D = P/C$  is the heat diffusion coefficient.  $K_T^{-1}$ ,  $K_R^{-1}$ , and  $K_{EF}^{-1}$  are numerical constant parameters that weigh each term in the objective function and control its rate of convergence. Following Bateni et al. (2013a),  $K_T^{-1}$ ,  $K_R^{-1}$ , and  $K_{EF}^{-1}$  are set to  $0.01 \text{ K}^{-2}$ , 1000, and 1000, respectively.

The optimal values for  $C_{HN}$  and  $EF$  are found by minimizing the cost function. To minimize the cost function, its first variation should be set to zero ( $\Delta J = 0$ ) (Bennett, 1992). Setting  $\Delta J$  to zero leads to a number of Euler-Lagrange equations that should be solved simultaneously through an iterative loop to obtain optimal values of  $C_{HN}$  and  $EF$ . The Euler-Lagrange equations for the CS VDA scheme can be found in Bateni et al. (2013a).

Similarly,  $C_{HN}$ ,  $EF_S$  and  $EF_C$  are estimated by minimizing the difference between the GOES LST and the effective LST estimates (Eq. 10). The cost function for the DS model is defined as,

$$\begin{aligned}
J(T, R, EF_S, EF_C, \lambda) = & \\
& \sum_{i=1}^N \int_{t_0}^{t_1} [T_{OBS,i}(t) - T_i(t)]^T K_T^{-1} [T_{OBS,i}(t) - T_i(t)] dt \\
& + (R - R')^T K_R^{-1} (R - R') + \sum_{i=1}^N (EF_{S,i} - EF'_{S,i})^T K_{EF_S}^{-1} (EF_{S,i} - EF'_{S,i}) \\
& + \sum_{i=1}^N (EF_{C,i} - EF'_{C,i})^T K_{EF_C}^{-1} (EF_{C,i} - EF'_{C,i}) \\
& + 2 \sum_{i=1}^N \int_{t_0}^{t_1} \int_0^l \lambda_i(z, t) \left[ \frac{\partial T_{S,i}(z, t)}{\partial t} - D \frac{\partial T_{S,i}^2(z, t)}{\partial z^2} \right] dz dt
\end{aligned} \tag{12}$$

where the third and fourth terms on the right-hand side of Eq. (12) measures the difference between the soil and canopy evaporative fraction estimates and their prior values, respectively.  $K_T^{-1}$ ,  $K_R^{-1}$ ,  $K_{EF_S}^{-1}$ , and  $K_{EF_C}^{-1}$  are respectively set to  $0.01 \text{ K}^{-2}$ , 1000, 1000, and 1000 based on Bateni and Liang (2012).

In the DS VDA scheme, the optimal values for  $C_{HN}$ ,  $EF_S$  and  $EF_C$  are found by minimizing the cost function (Eq. 12). Setting  $\Delta J$  to zero yields a number of Euler-Lagrange equations as follows:

$$\frac{\partial \lambda}{\partial t} + D \frac{\partial^2 \lambda}{\partial z^2} = 0 \tag{13a}$$

$$\lambda(z, t_1) = 0 \quad (13b)$$

$$\begin{aligned} \left. \frac{\partial \lambda}{\partial z} \right|_{z=0} &= \frac{K_T^{-1}}{D} (T - T_{OBS}) (1 - f_C) T_S^3 T^{-3} \\ &+ \frac{\lambda(0, t)}{P} \left[ 4\varepsilon_s \sigma T_S^3 + \frac{\rho c_p e^R f(Ri) U \exp(-a_H LAI)}{1 - EF_S} \right] (1 - f_C) \end{aligned} \quad (13c)$$

$$\left. \frac{\partial \lambda}{\partial z} \right|_{z=l} = 0 \quad (13d)$$

$$\begin{aligned} R &= R' - \frac{1}{CK_R^{-1}} \sum_{i=1}^N \int_{t_0}^{t_1} \lambda_i(0, t) \left[ \frac{\rho c_p e^R f(Ri) U \exp(-a_H LAI) (T_S - T_W)}{1 - EF_{S,i}} \right] (1 - f_C) dt \\ &- \frac{K_T^{-1}}{K_R^{-1}} \sum_{i=1}^N \int_{t_0}^{t_1} (T - T_{OBS}) \frac{\rho c_p e^R f(Ri) U \exp(-0.5 a_H LAI) (T_W AA - BB)}{AA^2} f_C T_C^3 T^{-3} dt \end{aligned} \quad (14a)$$

$$EF_{S,i} = EF'_{S,i} - \frac{1}{CK_{EF_S}^{-1}} \int_{t_0}^{t_1} \frac{\lambda(0, t)}{(1 - EF_{S,i})^2} \rho c_p e^R f(Ri) U \exp(-a_H LAI) (T_S - T_W) (1 - f_C) dt \quad (14b)$$

$$EF_{C,i} = EF'_{C,i} - \frac{K_R^{-1}}{K_{EF_C}^{-1}} \int_{t_0}^{t_1} \frac{4\varepsilon_s \sigma T_A^3 BB - [(1 - \alpha_C) R_S^\downarrow + R_L^\downarrow + 3\varepsilon_s \sigma T_A^4] AA}{AA^2} f_C T_C^3 T^{-3} (T - T_{OBS}) \quad (14c)$$

where  $AA = 4\varepsilon_s \sigma T_A^3 (1 - EF_C) + \rho c_p C_{HN} f(Ri) \exp(-0.5 a_H LAI) U$

$BB = [(1 - \alpha_C) R_S^\downarrow + R_L^\downarrow + 3\varepsilon_s \sigma T_A^4] (1 - EF_C) + \rho c_p C_{HN} f(Ri) \exp(-0.5 a_H LAI) U T_W$ ,  $\varepsilon_s$  is the soil emissivity (-),  $\sigma$  is the Stefan–Boltzmann constant ( $5.67 \times 10^{-8} \text{ W m}^{-2} \text{ K}^{-4}$ ), and  $R_S^\downarrow$  and  $R_L^\downarrow$  are the downward shortwave and longwave radiation ( $\text{W m}^{-2}$ ).

The adjoint model (Eq. [13a]) has to be integrated backward in time using the terminal and boundary conditions (Eqs. [13b], [13c], and [13d]). The unknown parameters of the DS scheme (i.e.,  $R$ ,  $EF_S$ , and  $EF_C$ ) can be estimated via Eqs. (14a), (14b) and (14c). The DS VDA scheme improves estimates of the three unknown parameters iteratively starting from the initial guesses ( $R'$ ,  $EF'_S$ , and  $EF'_C$ ).

## Principal Findings and Significance

### Neutral Heat Transfer Coefficient and Evaporative Fraction

As mentioned in the previous section,  $C_{HN}$  and  $EF$  are the two key unknown parameters in the CS model, and  $C_{HN}$ ,  $EF_S$  and  $EF_C$  constitute the three unknown parameters in the DS model.  $C_{HN}$  and  $EF$  are estimated on monthly and daily timescales, respectively. In the VDA framework,

the accuracy of turbulent heat flux estimates mainly depends on the robust retrieval of these unknown parameters.

The estimated  $C_{HN}$  values from the CS and DS schemes for the six experimental sites are shown in Table 1.  $C_{HN}$  estimates from the CS and DS models have generally the same order of magnitude and are comparable with each other over different assimilation periods. However, in most cases, the DS  $C_{HN}$  values are slightly larger than those of the CS model. The discrepancy between  $C_{HN}$  estimates from the CS and DS schemes is due to the difference in the structure of the CS and DS schemes. To understand this distinction better, the  $C_{HN}$  estimates from the CS,  $(C_{HN})_{CS}$ , and DS,  $(C_{HN})_{DS}$ , schemes are related using Eqs. (4) and (8a):

$$(C_{HN})_{DS} = (C_{HN})_{CS} \frac{T - T_A}{T_W - T_A} \quad (15)$$

The land surface temperature ( $T$ ) is usually larger than the air temperature within the canopy ( $T_W$ ) during the assimilation window (i.e.,  $T > T_W$ ). Subtracting  $T_A$  from both sides of the inequality leads to  $(T - T_A) > (T_W - T_A)$ . Thus, the  $C_{HN}$  estimates from the DS scheme should typically be higher than those from the CS scheme (see Table 1).

Table 1. Summary of the Characteristics Over Six Study Sites

Site	Land Cover	LAI ( $m^2 m^{-2}$ )	$f_C$	SM ( $m^3 m^{-3}$ )	$C$ ( $J m^{-3} K^{-1}$ )	$P$ ( $J m^{-1} K^{-1} s^{-1}$ )
Brookings	Grassland	1.6	0.55	0.43	$3.04 \times 10^6$	1.64
Goodwin	Grassland	1.8	0.59	0.31	$2.57 \times 10^6$	1.75
Bondville	Cropland	2.7	0.74	0.32	$2.58 \times 10^6$	1.55
Mead	Cropland	1.8	0.59	0.25	$2.58 \times 10^6$	1.54
Chestnut	Forest	5.4	0.93	0.19	$2.06 \times 10^6$	1.53
Missouri	Forest	5.4	0.93	0.30	$2.53 \times 10^6$	1.70

LAI values over different periods are listed in Table 2 to explore the relationship between  $C_{HN}$  estimates and vegetation phenology. The  $C_{HN}$  estimates generally increase with LAI values at each site. Remarkably, the  $C_{HN}$  estimates from both schemes are higher at sites with larger LAI values (i.e., Chestnut and Missouri) (Table 1), implying that the VDA system can robustly retrieve  $C_{HN}$  from sequences of LST observations. This is particularly interesting because no information on vegetation phenology is used in the CS model. Yet, its  $C_{HN}$  estimates are larger at sites with denser canopies.

Table 2. Neutral Bulk Heat Transfer Coefficient Estimates from the CS and DS Models

	Day of Year	Brookings	Goodwin	Bondville	Mead	Chestnut	Missouri
CS	151–180	$1.0 \times 10^{-2}$	$1.1 \times 10^{-2}$	$0.6 \times 10^{-2}$	$1.7 \times 10^{-2}$	$8.7 \times 10^{-2}$	$5.7 \times 10^{-2}$
	181–210	$1.0 \times 10^{-2}$	$1.5 \times 10^{-2}$	$1.3 \times 10^{-2}$	$1.9 \times 10^{-2}$	$10.0 \times 10^{-2}$	$8.7 \times 10^{-2}$
	211–240	$1.4 \times 10^{-2}$	$1.5 \times 10^{-2}$	$1.1 \times 10^{-2}$	$2.1 \times 10^{-2}$	$8.9 \times 10^{-2}$	$10.9 \times 10^{-2}$
DS	151–180	$1.3 \times 10^{-2}$	$1.3 \times 10^{-2}$	$1.1 \times 10^{-2}$	$2.3 \times 10^{-2}$	$8.9 \times 10^{-2}$	$6.1 \times 10^{-2}$
	181–210	$1.6 \times 10^{-2}$	$1.5 \times 10^{-2}$	$1.5 \times 10^{-2}$	$2.0 \times 10^{-2}$	$11.5 \times 10^{-2}$	$9.8 \times 10^{-2}$
	211–240	$1.8 \times 10^{-2}$	$1.6 \times 10^{-2}$	$1.3 \times 10^{-2}$	$2.2 \times 10^{-2}$	$7.9 \times 10^{-2}$	$11.1 \times 10^{-2}$
LAI	151–180	1.2	1.7	1.5	1.4	5.0	5.3
	181–210	1.7	2.0	4.0	2.0	5.8	5.6
	211–240	2.0	1.6	2.5	2.0	5.4	5.4

<sup>a</sup>LAI represents the leaf area index.

Figure 1 shows the time series of the evaporative fraction ( $EF$ ) values estimated from the CS and DS schemes. For comparison,  $EF$  observations are also shown on the same figure. The estimated  $EF$  values from the CS and DS models agree well with the observations in terms of both magnitude and day-to-day dynamics. Additionally, the DS model yields  $EF$  values closer to observations than the CS model. Oscillations in the estimated  $EF$  values are consistent with land surface wetting and drying events.  $EF$  values increase sharply when precipitation happens and reduce in drydown periods even though no soil moisture or precipitation data are used in the model. For example, during the drydown period at the Brookings (Julian day 171 to 191), Goodwin (Julian day 191 to 211) and Missouri (Julian day 191 to 221) sites,  $EF$  estimates decrease significantly.

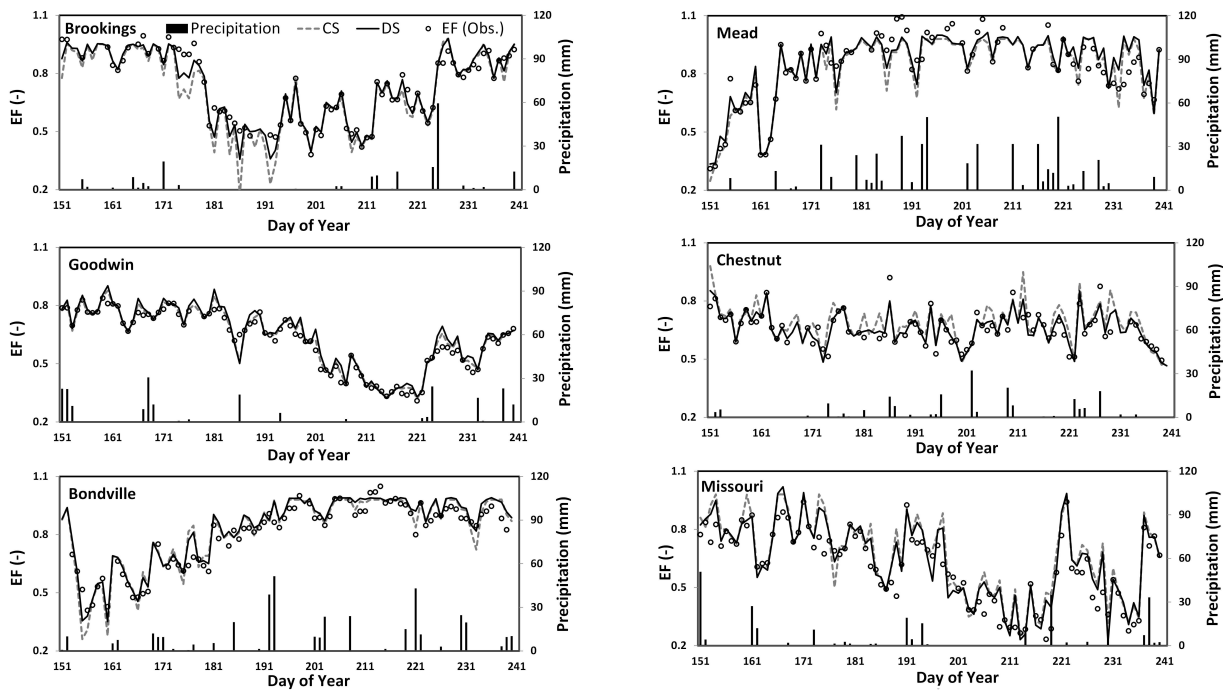


Figure 1. Time series of evaporative fraction ( $EF$ ) estimates from the CS and DS models.

## Sensible and Latent Heat Fluxes

Figure 2 compares the half-hourly turbulent heat flux estimates from the CS and DS models with the corresponding measurements at the Brookings, Goodwin, Bondville, Mead, Chestnut, and Missouri sites. This figure allows us to evaluate the performance of the CS and DS models in different hydrological and vegetative conditions. As shown, the sensible and latent heat fluxes retrieved from both models are in good agreement with the observations and mainly fall around the 1:1 line. Additionally, the DS scheme performs better than the CS scheme. This is because the DS model can represent the physics of the problems more robustly. The misfits between the model estimates and observations are mainly due to the physical assumptions (constant soil thermal conductivity ( $P$ ) and heat capacity ( $C$ ), constant daily  $EF$ ,  $EF_C$ ,  $EF_S$ , constant monthly  $C_{HN}$ ) in the CS and DS models. Over the Goodwin and Chestnut sites, both the CS and DS schemes tend to overestimate latent heat flux when it is larger than  $200 \text{ W m}^{-2}$ . This may be due to the undermeasurement of sensible and latent heat fluxes by the Eddy Covariance

(EC) technique, i.e., the so-called “energy imbalance” problem. The energy balance ratio ( $EBR = (H+LE)/(R_N-G)$ ) is 0.78 and 0.75 at the Goodwin and Chestnut sites, respectively, implying that the EC method underestimates the latent heat flux. This leads to a bias greater than  $60 \text{ W m}^{-2}$  in the  $LE$  estimates at these two sites.

The bias and root-mean-square error (RMSE) of the turbulent heat flux estimates at the six experimental sites are shown in Figure 2 as well. For sensible heat flux, the six-site-averaged bias and RMSE (shown in parenthesis) from the CS and DS schemes are 7.5 (59.7) and 1.7 (52.5)  $\text{Wm}^{-2}$ , respectively. For latent heat flux, the six-site-averaged bias (RMSE) is 19.0 (111.1)  $\text{Wm}^{-2}$  for the CS scheme and 12.7 (96.4)  $\text{Wm}^{-2}$  for the DS scheme. The low bias and RMSE values imply that the CS and DS schemes can retrieve turbulent heat fluxes accurately.

By treating the soil and the canopy as different sources and accounting for their interaction with the overlying atmosphere in the DS model, the bias (RMSE) of retrieved sensible and latent heat fluxes over the six experimental sites is on average 77% and 33% (12% and 13%) less than that of the CS model. Overall, the statistical metrics in Figure 2 indicate that decomposing the land surface into canopy and soil sources via the DS model improves the estimate of turbulent heat fluxes.

The discrepancies between the results of the CS and DS models are mainly due to the different model structures. The DS model treats the soil and vegetation canopy as dual sources, while the CS model treats them as combined sources. The DS model can characterize the heterogeneity of the land surface and weighs the soil and canopy fluxes via the vegetation cover fraction ( $f_C$ ) (see Eq. 8b), while the less elaborate CS scheme cannot. The  $f_C$  values for the six sites are listed in Table 1. As shown in Figure 2, the largest discrepancy between the CS and DS turbulent heat flux estimates occurs when  $f_C$  is approximately 0.5–0.6 (at the Goodwin and Mead sites). When  $f_C$  is about 0.5, the land surface heterogeneity is at its peak, and thus the CS model cannot capture the physics of the underlying problem as robustly as the DS model. As a result, the maximum difference is observed between the CS and DS scheme  $H$  and  $LE$  estimates (see Table 3). As  $f_C$  increases to 0.7 (at the Bondville site), land surface patchiness decreases, and therefore the misfit between the CS and DS model retrievals decreases (Table 3). At an  $f_C$  of about 0.9 (at the Chestnut and Missouri sites), land surface patchiness reaches its minimum because the land surface is mainly composed of canopy. Consequently, the CS model can retrieve turbulent heat fluxes almost as accurately as the DS model. Turbulent heat fluxes are mainly controlled by atmospheric factors rather than land surface properties at the Brookings site since it is a wet site. Therefore, even with an  $f_C$  value of 0.55 at this site (i.e., high land surface heterogeneity), a small discrepancy is found between the CS and DS model estimates (Table 3). At the Bondville site,  $f_C$  illustrates a pronounced seasonal variation and increases from 0.53 (for Julian days 151–180) to 0.86 (for Julian days 181–210). As a result, the discrepancy between turbulent flux estimates from the CS and DS model is higher for Julian days 151–180 compared to Julian days 181–210 (see Table 3).

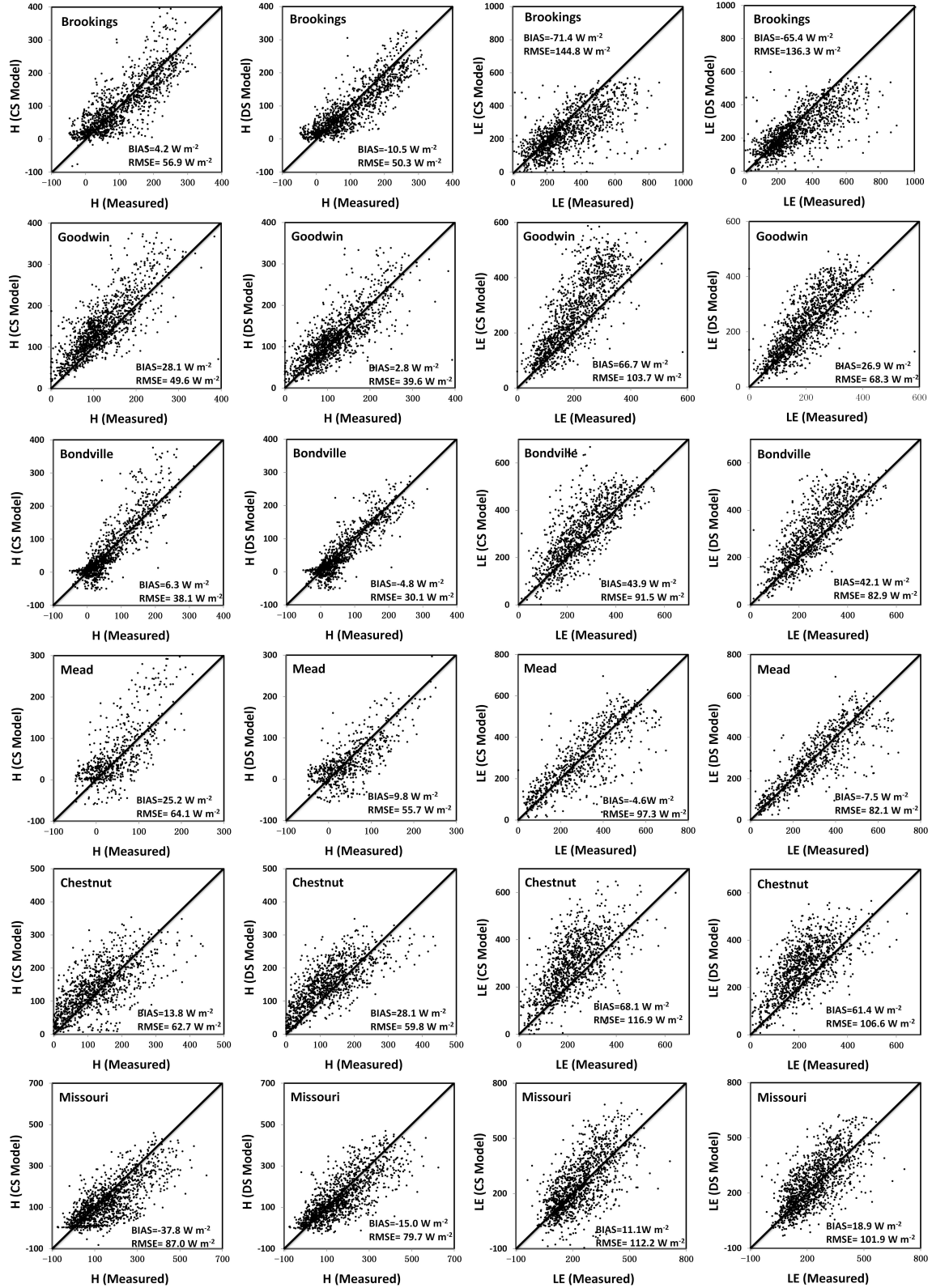


Figure 2. Scatterplots between modeled (CS and DS) and measured (EC data) sensible and latent heat fluxes ( $H$  and  $LE$ ) in the six sites for Julian days 151–240 in 2006.

Table 3. The Percentage Relative Difference of Turbulent Heat Flux Estimates from the CS and DS Schemes

	Day of Year	Brookings	Goodwin	Bondville	Mead	Chestnut	Missouri
$P_H$ (%)	151–180	–20.4	–23.7	–14.3	–28.4	6.3	9.6
	181–210	–5.2	–15.9	–11.5	–24.5	9.7	14.4
	211–240	–7.7	–15.1	–22.5	–21.1	14.6	14.2
	151–240	–11.1	–18.2	–16.1	–24.7	10.2	12.7
$P_{LE}$ (%)	151–180	3.7	18.7	10.7	11.3	–5.2	–3.1
	181–210	7.7	11.4	0.5	3.5	–2.2	–4.3
	211–240	1.4	12.8	4.6	3.9	–1.1	–2.4
	151–240	4.2	14.3	5.3	6.2	–2.8	–3.3
$f_C$	151–180	0.45	0.57	0.53	0.50	0.92	0.93
	181–210	0.57	0.63	0.86	0.63	0.94	0.94
	211–240	0.63	0.55	0.71	0.63	0.93	0.93
	151–240	0.55	0.59	0.74	0.59	0.93	0.93

<sup>a</sup> $P_H(\%) = (H_{(DS)} - H_{(CS)})/H_{(CS)} \times 100$  and  $P_{LE}(\%) = (LE_{(DS)} - LE_{(CS)})/LE_{(CS)} \times 100$ .  $H_{(CS)}$  and  $H_{(DS)}$  represent the sensible heat flux estimates from the CS and DS schemes,  $LE_{(CS)}$  and  $LE_{(DS)}$  denote the latent heat flux estimates from the CS and DS schemes, and  $f_C$  means vegetation cover fraction.

Figure 3 shows the time series of daytime-averaged (0900–600 LT) estimated sensible and latent heat fluxes from the CS and DS models at the six experimental sites. Results from control experiments (i.e., without assimilation of GOES LST) and EC observations are indicated in Figure 3. The CS and DS model estimates are consistent with the observations in terms of both magnitude and day-to-day dynamics, implying that assimilating LST data from GOES can reliably partition the available energy among sensible and latent heat fluxes. However, the turbulent heat flux estimates degrade in wet periods (e.g., Julian days 151–180 at the Brookings site and Julian days 201–215 at the Mead site). At the Brookings and Mead sites (data for Mead shown in parenthesis), the daytime-averaged latent heat flux measurements increase to approximately  $700 \text{ Wm}^{-2}$  ( $600 \text{ Wm}^{-2}$ ) in the corresponding aforementioned wet periods, while the model estimates cannot reach those high values. This happens because the upper bound of  $EF$  (i.e.,  $EF_S$  and  $EF_C$ ) in the CS (DS) model is set to 0.97 to avoid numerical instabilities, while the corresponding  $EF$  observations are sometimes larger than 1.0 due to negative sensible heat flux measurements (according to Eq. [5], negative sensible heat flux measurements lead to  $EF$  values larger than 1.0).

As indicated in Figure 3, the estimated  $H$  and  $LE$  values from the VDA models are closer to the observations than those of the control experiments. The good agreement between the estimated and observed turbulent heat fluxes illustrates that the VDA model can effectively use implicit information in the LST observations to constrain the unknowns of the CS and DS schemes. In contrast, the control experiments perform poorly since there is no constraint by the LST observations.

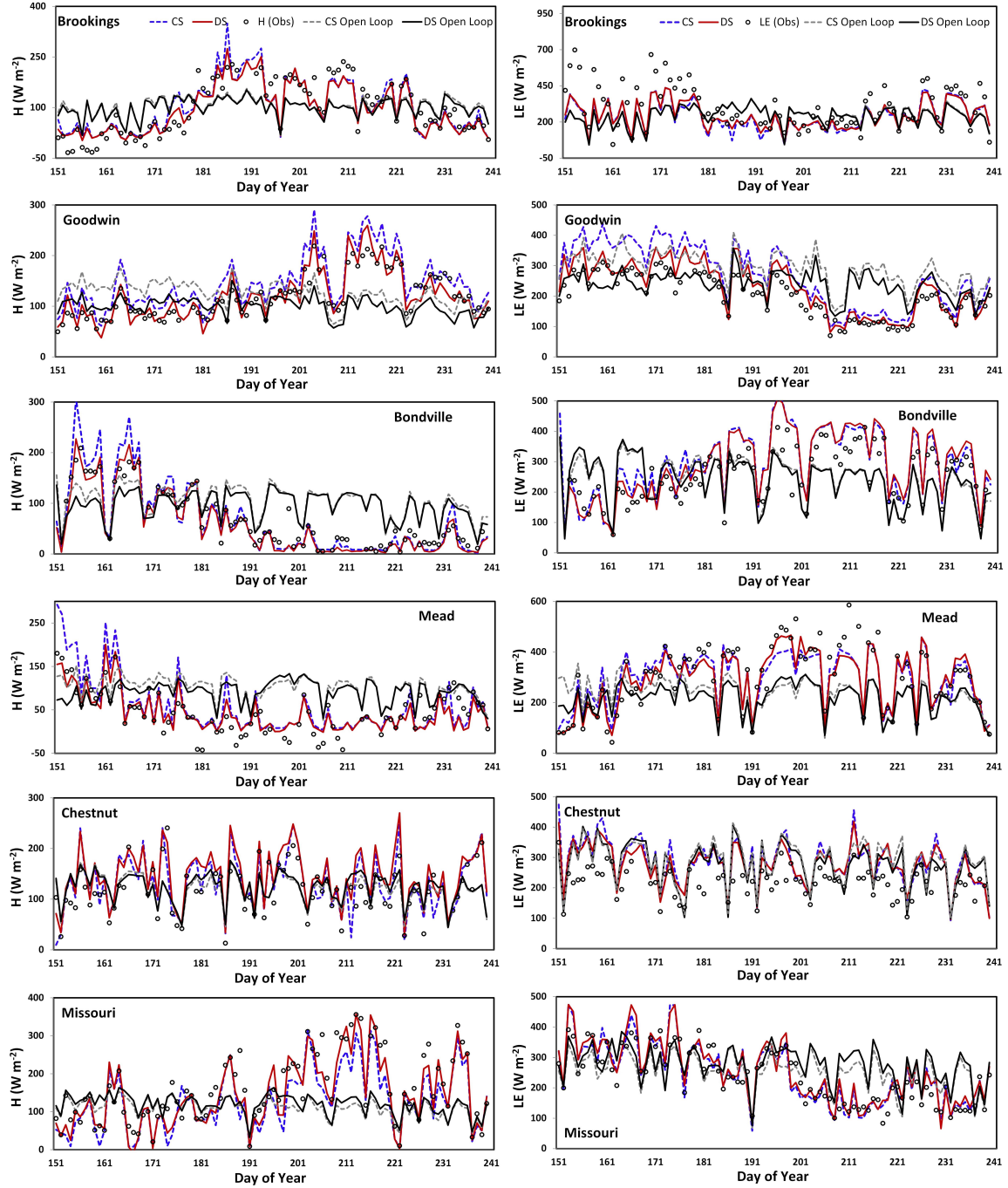


Figure 3. Time series of daytime-averaged sensible and latent heat flux ( $H$  and  $LE$ ) estimates in the six experimental sites from the CS scheme with (blue dashed lines) and without (grey dashed lines) assimilation of GOES LST. Corresponding estimates from the DS scheme with (red solid lines) and without (black solid lines) assimilation of GOES LST. Observations are shown by open circles.

Figure 4 shows the mean diurnal cycle of observed and estimated turbulent heat fluxes from the CS and DS models at the six experimental sites. As indicated, the diurnal variations of retrieved turbulent heat fluxes from both models agree well with those of observations in terms of magnitude and phase. A large discrepancy between the CS and DS model diurnal cycles is found at the Goodwin ( $f_C = 0.59$ ) and Mead ( $f_C = 0.59$ ) sites, which have high land surface

heterogeneity. In contrast, at sites in which the land surface tends to be more homogeneous (e.g., Bondville, Chestnut, and Missouri, with  $f_C$  of 0.74, 0.93, and 0.93, respectively), the diurnal cycle retrievals from the CS and DS scheme are close. At the Chestnut site, the CS and DS models overestimate both the sensible and latent heat fluxes. This is mainly because turbulent heat flux measurements from the EC system at the Chestnut site may contain errors and suffer from the “energy imbalance” problem. Overall, the misfit between the observed and estimated diurnal cycles is due to a number of reasons, including the assumptions of constant daily evaporative fraction and constant monthly neutral bulk heat transfer coefficient and the use of constant soil thermal properties over the modeling period.

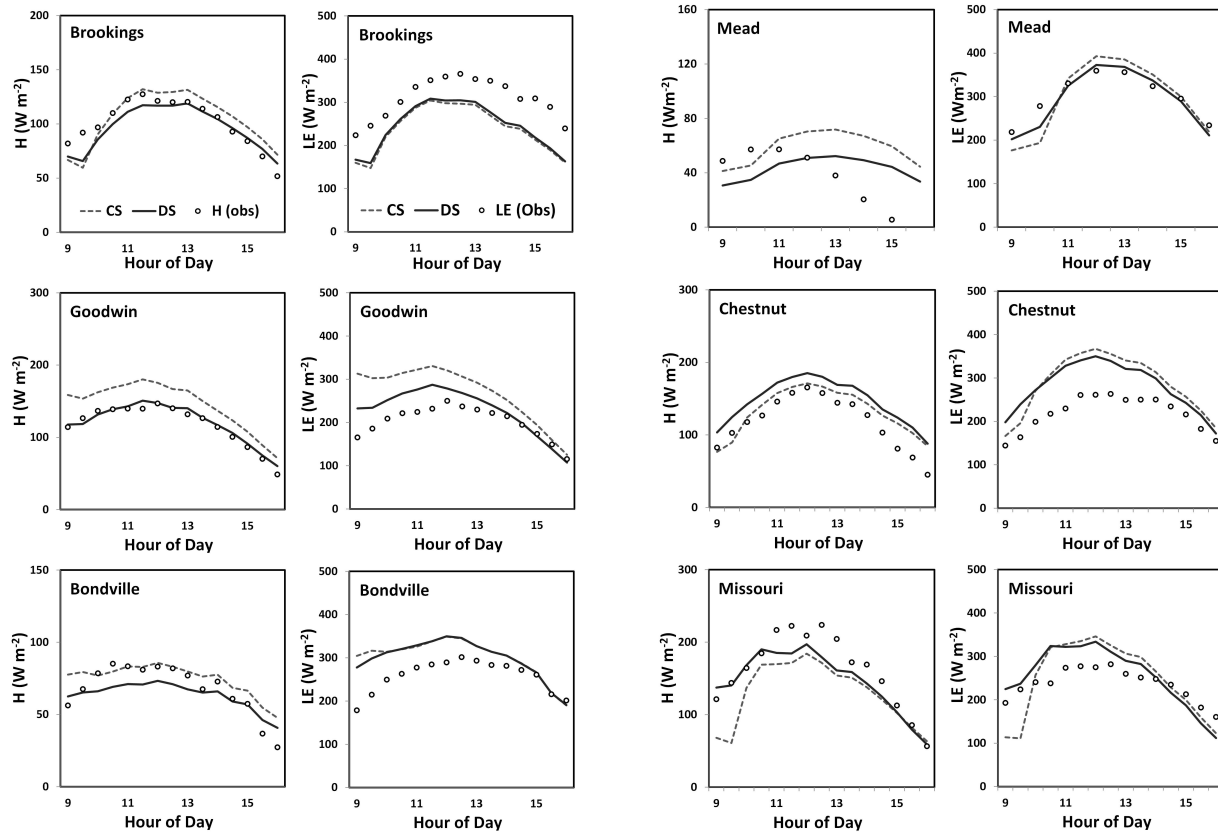


Figure 4. Mean diurnal cycle of turbulent heat flux estimates from the CS and DS models along with the observations in the six experimental sites (H and LE mean sensible and latent heat fluxes).

Figure 5 shows the relationship between RMSE of turbulent heat flux estimates and its soil moisture and vegetation cover fraction, at each of the six explored sites. Each circle corresponds to a site and its size represents the RMSE of flux estimates at the site (larger circles illustrate higher RMSE values). As indicated, the CS and DS models perform better at dry and/or sparsely vegetated sites than at wet and/or densely vegetated sites. Similarly, the results in Figure 2 indicate that the CS and DS schemes yield larger biases and RMSE values (less accurate turbulent heat fluxes) over densely vegetated/wet sites than over lightly vegetated/dry sites. For example, the bias and RMSE of turbulent heat flux estimates at the Chestnut and Missouri sites with denser vegetation cover (i.e., higher LAI value) are larger than those at the Goodwin, Bondville, and Mead sites with lower canopy cover. Additionally, at the Brookings site, which

has higher soil moisture, the turbulent heat flux retrievals degrade compared to the drier Goodwin, Bondville, and Mead sites.

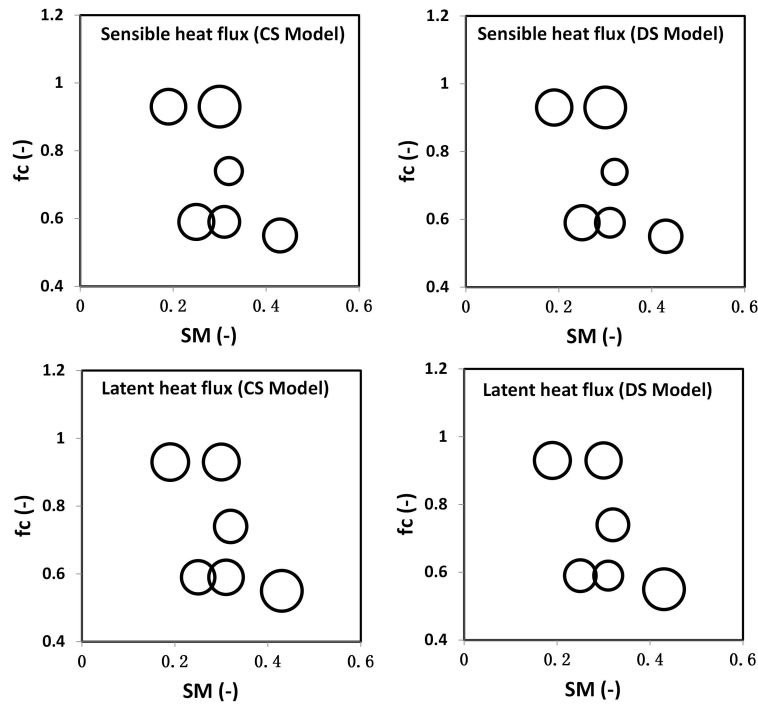


Figure 5. The relationship between the RMSE of turbulent heat flux estimates at each site and its soil moisture (SM) and vegetation cover fraction ( $f_c$ ). Circle size is determined by the RMSE of flux estimates at each site (larger circles indicate higher RMSE values).

In another study, Crow and Kustas (2005) tested only the CS VDA system with the force-restore equation as an adjoint (VDA-FR) over a range of vegetative and hydrological conditions in the southern U.S. They found that performance of the CS VDA-FR framework degraded over densely vegetated and/or wet sites, and suggested additional land surface information (e.g., leaf area index, LAI) is required to accurately predict surface heat fluxes in densely vegetated and wet sites. In comparison to the Crow and Kustas (2005) study, this project tested both the CS and DS VDA systems with the full heat diffusion equation (instead of the parsimonious force-restore equation) over six sites across the USA. Since even the DS scheme (that uses LAI) cannot perform robustly in densely vegetated/wet sites, it is suggested to assimilate soil moisture or rainfall observations within the VDA scheme in future studies.

### Impact of Climate Change on Surface Heat Fluxes

In addition to LST, which lies at the heart of the surface energy balance equation and has information on the partitioning of available energy among the surface energy balance components (Bateni and Entekhabi, 2012a, 2012b), LAI variations (used only in the DS model) control this partitioning (Segal et al., 1988; Alfieri et al., 2009; Bateni et al., 2013b). In this section, a number of sensitivity tests are performed to understand the impact of changes in LST and LAI on the surface turbulent flux estimates. The main goal of sensitivity tests is to provide insights into the effect of variations in LST and LAI (due to climate change) on the heat fluxes.

The Bondville site is selected for this purpose in this study. In the first set of tests, LST observations are varied by  $\pm 2$ ,  $\pm 4$ ,  $\pm 6$ ,  $\pm 8$ , and  $\pm 10$  K from their nominal values and are used in the CS and DS schemes to estimate turbulent heat fluxes. Figure 6 shows the sensitivity of  $H$  and  $LE$  estimates from the CS and DS schemes to uncertainties in LST. For the CS approach, increasing LST by 2, 4, 6, 8, and 10 K leads to a 13.0%, 18.3%, 23.0%, 33%, and 37.8% reductions in  $H$  and a 10.9%, 22.8%, 32.1%, 39.9%, and 46.9% increase in  $LE$ . On the other hand, decreases in LST by 2, 4, 6, 8, and 10 K causes  $H$  to be decreased by 12.4%, 27.5%, 40.1%, 48.8%, and 55.1%, and causes  $LE$  to be increased by 9.9%, 17.9%, 22.9%, 26.1%, and 28.3%.

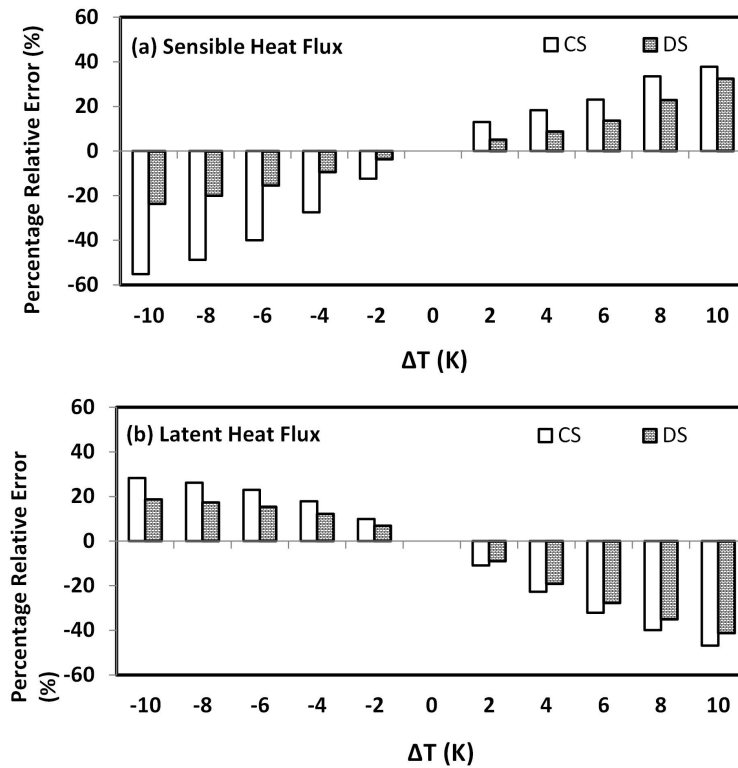


Figure 6. The percentage relative error of estimated sensible heat flux by different sensitivity tests accounting for variations in LST. The original run sensible heat flux estimates are obtained by the CS and DS models with nominal LST observations at the Bondville site.

As indicated in Figure 6, the estimated turbulent heat fluxes from the DS scheme are less sensitive to uncertainties in LST (i.e., the DS model performs better than the CS model when biased LST data are assimilated). For example,  $H$  and  $LE$  estimates vary 13.6% and 27.8% as LST becomes 6 K larger than its nominal value.

To assess the effect of variations in LAI on the sensible and latent heat flux estimates, the nominal LAI values are varied by  $\pm 20\%$ ,  $\pm 50\%$ , and  $\pm 100\%$  and are used in the DS model. Since the CS model does not use LAI, the sensitivity tests herein are performed with the DS approach only. The sensitivity of estimated sensible and latent heat flux to variations in LAI is indicated in Figure 7. Decreasing LAI by 20%, 50%, and 100% yields a 4.2%, 8.1%, and 13.1% increase in sensible heat flux and a 3.8%, 8.0%, and 18.1% reduction in latent heat flux. Also, the DS model tends to yield larger errors when fed with underestimated leaf area index values. Overall, all of

these results clearly demonstrate that the correct specification of LST and LAI play an important role in the accurate retrieval of turbulent heat fluxes. These findings also allow us to quantitatively characterize the effect of uncertainties in LST and LAI on the turbulent heat flux estimates.

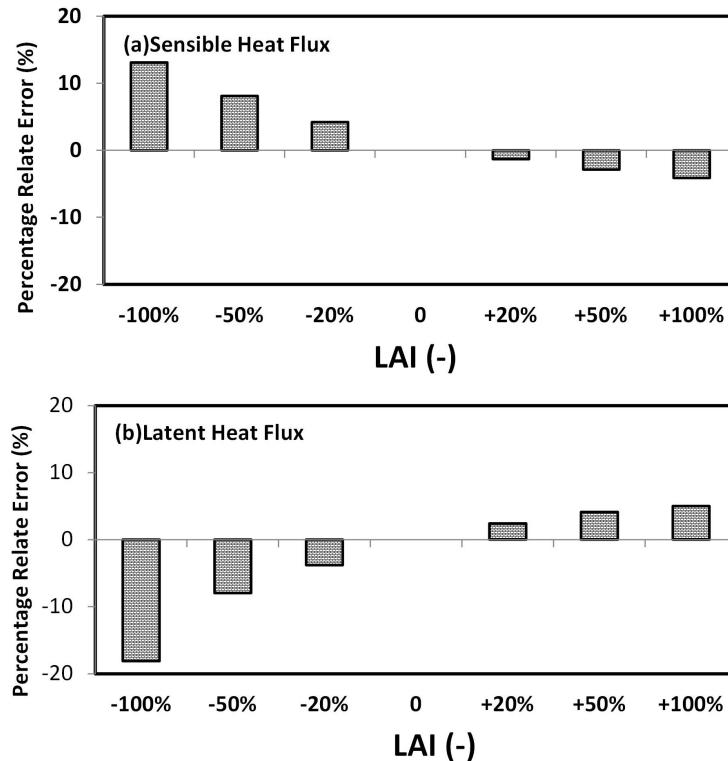


Figure 7. (a) The percentage relative error of estimated sensible heat flux by different sensitivity tests accounting for changes in leaf area index (LAI). The original run sensible heat flux estimates are obtained by the CS and DS models with the nominal LAI observations, (b) The same as in Figure 7a but for latent heat flux.

## Publication Cited in Synopsis

- Alfieri, J.G., X. Xiao, D. Niyogi, Sr., R.A. Pielke, F. Chen, and M.A. Lemone, 2009, "Satellite-based modeling of transpiration from the grasslands in southern great plains, USA," *Global Planet Change*, 67(1–2), 78–86.
- Anderson, M.C., J.M. Norman, G.R. Diak, W.P. Kustas, , and J.R. Mecikalski, 1997, "A two-source time-integrated model for estimating surface fluxes using thermal infrared remote sensing," *Remote Sensing of Environment*, 60(2), 195–216.
- Bastiaanssen, W.G.M., M. Menenti, R. Feddes, and A. Holtslag, 1998a, "A remote sensing surface energy balance algorithm for land (SEBAL): 1. Formulation," *Journal of Hydrology*, 212, 198–212.
- Bastiaanssen, W.G.M., H. Pelgrum, J. Wang, Y. Ma, J. Moreno, G. Roerink, and T. Van der Wal, 1998b, "A remote sensing surface energy balance algorithm for land (SEBAL): Part 2: Validation," *Journal of Hydrology*, 212, 213–229.

- Bateni, S.M., and D. Entekhabi, 2012a, "Relative efficiency of land surface energy balance components," *Water Resources Research*, 48(8).
- Bateni, S.M., and D. Entekhabi, 2012b, "Relative efficiency of land surface energy balance components," *Water Resources Research*, 48(4).
- Bateni, S.M., D. Entekhabi, and F. Castelli, 2013a, "Mapping evaporation and estimation of surface control of evaporation using remotely sensed land surface temperature from a constellation of satellites," *Water Resources Research*, 49(2), 950–968.
- Bateni, S.M., D. Entekhabi, and D. S. Jeng, 2013b, "Variational assimilation of land surface temperature and the estimation of surface energy balance components," *Journal of Hydrology*, 481, 143–156.
- Bateni, S.M., D.S. Jeng, and S.M. Mortazavi Naeini, 2012, "Estimating soil thermal properties from sequences of land surface temperature using hybrid Genetic Algorithm-Finite Difference method," *Engineering Applications of Artificial Intelligence*, 25(7), 1425–1436.
- Bateni, S.M., and S. Liang, 2012, "Estimating surface energy fluxes using a dual-source data assimilation approach adjoined to the heat diffusion equation," *Journal of Geophysical Research: Atmospheres* (1984–2012), 117(D17).
- Bennett, A.F., 1992, *Inverse Methods in Physical Oceanography*, Cambridge, New York, Cambridge University Press, 368 p.
- Boni, G., D. Entekhabi, and F. Castelli, 2001, "Land data assimilation with satellite measurements for the estimation of surface energy balance components and surface control on evaporation," *Water Resources Research*, 37(6), 1713–1722.
- Caparrini, F., F. Castelli, and D. Entekhabi, 2003, "Mapping of land-atmosphere heat fluxes and surface parameters with remote sensing data," *Boundary-layer Meteorology*, 107(3), 605–633.
- Caparrini, F., F. Castelli, and D. Entekhabi, 2004a, "Estimation of surface turbulent fluxes through assimilation of radiometric surface temperature sequences," *Journal of Hydrometeorology*, 5, 145–159.
- Caparrini, F., F. Castelli, and D. Entekhabi, 2004b, "Variational estimation of soil and vegetation turbulent transfer and heat flux parameters from sequences of multisensor imagery," *Water Resources Research*, 40, 1713–1722.
- Castelli, F., D. Entekhabi, and E. Caporali, 1999, "Estimation of surface heat transfer and an index of soil moisture using adjoint-state surface energy balance," *Water Resources Research*, 35, 3115–3126.
- Crow, W.T., and W.P. Kustas, 2005, "Utility of assimilating surface radiometric temperature observations for evaporative fraction and heat transfer coefficient retrieval," *Boundary-layer Meteorology*, 115(1), 105–130.
- Gentine, P., D. Entekhabi, and A. Chehbouni, 2007, "Analysis of evaporative fraction diurnal behavior," *Agricultural and Forest Meteorology*, 143(1–2).
- Hu, Z., and S. Islam, 1995, "Prediction of ground temperature and soil moisture content by the force-restore method," *Water Resources Research*, 31(10).
- Jensen, N.O., and P. Hummelshøj, 1995, "Derivation of canopy resistance for water vapor fluxes over a spruce forest, using a new technique for the viscous sublayer resistance," *Agriculture and Forest Meteorology*, 73, 339–352.
- Jia, L., G. Xi, S. Liu, C. Huang, Y. Yan, and G. Liu, 2009, "Regional estimation of daily to annual regional evapotranspiration with MODIS data in the Yellow River Delta wetland," *Hydrology and Earth System Sciences*, 13, 1775–1787.

- Jiang, L., and S. Islam, 2001, "Estimation of surface evaporation map over Southern Great Plain using remote sensing data," *Water Resources Research*, 37(2), 329–340.
- Jiang, L., and S. Islam, 2003, "An intercomparison of regional latent heat flux estimation using remote sensing data," *International Journal of Remote Sensing*, 24(11), 2221–2236.
- Kustas, W.P., K.S. Humes, J.M. Norman, and M.S. Moran, 1996, "Single and dual-source modeling of surface energy fluxes with radiometric surface temperature," *Journal of Applied Meteorology and Climatology*, 35(1), 110–121.
- Liu, S.M., G. Hu, L. Lu, and D. Mao, 2007, "Estimation of regional evapotranspiration by TM/ETM+ data over heterogeneous surfaces," *Photogrammetric Engineering and Remote Sensing*, 73, 1169–1178.
- Liu, S.M., Z.W. Xu, W.Z. Wang, Z.Z. Jia, M.J. Zhu, J. Bai, and J.M. Wang, 2011, "A comparison of eddy-covariance and large aperture scintillometer measurements with respect to the energy balance closure problem," *Hydrology and Earth System Sciences*, 15, 1291–1306.
- Liu, S. M., Z. W. Xu, Z. L. Zhu, Z.Z. Jia, and M.J. Zhu, 2013, "Measurements of evapotranspiration from eddy-covariance systems and large aperture scintillometers in the Hai River Basin, China," *Journal of Hydrology*, 487, 24–38.
- Ma, W., M. Hafeez, U. Rabbani, H. Ishikawa, and Y. Ma, 2012, "Retrieved actual ET using SEBS model from Landsat-5 TM data for irrigation area of Australia," *Atmospheric Environment*, 59, 408–414.
- McNaughton, K.G., and B.J.J.M. Van den Hurk, 1995, "A Lagrangian revision of the resistors in the two-layer model for calculating the energy budget of a plant canopy," *Boundary Layer Meteorology*, 74, 261–288.
- Nishida K., R.R. Nemani, J.M. Glassy, and S.W. Running, 2003, "Development of an evapotranspiration Index from Aqua/MODIS for monitoring surface moisture status," *IEEE Geoscience and Remote Sensing*, 41(2), 493–500.
- Norman, J.M., W.P. Kustas, and K. Humes, 1995, "A two-source approach for estimation of soil and vegetation energy fluxes from observations of directional radiometric surface temperature," *Agricultural and Forest Meteorology*, 77(3), 263–293.
- Qin, J., S. Liang, R. Liu, H. Zhang, and B. Hu, 2007, "A weak-constraint based data assimilation scheme for estimating surface turbulent fluxes," *IEEE Geoscience and Remote Sensing Letters*, 4(4), 649–653.
- Qualls, R.J., and W. Brutsaert, 1996, "Evaluation of spatially distributed ground-based and remotely sensed data to estimate spatially distributed sensible heat fluxes," *Water Resources Research*, 32, 2489–2495.
- Segal, M., R. Avissar, M.C. McCumber, and R.A. Pielke, 1988, "Evaluation of vegetation effects on the generation and modification of meso-scale circulations," *Journal of Atmospheric Sciences*, 45(16), 2268–2293.
- Sini, F., G. Boni, F. Caparrini, and D. Entekhabi, 2008, "Estimation of large-scale evaporation fields based on assimilation of remotely sensed land temperature," *Water Resources Research*, 44.
- Su, Z., 2002, "The Surface Energy Balance System (SEBS) for estimation of turbulent heat fluxes," *Hydrology and Earth System Science*, 6, 85–100.
- Sun, L., S. Liang, W. Yuan, and Z. Chen, 2013, "Improving a Penman–Monteith evapotranspiration model by incorporating soil moisture control on soil evaporation in semiarid areas," *International Journal of Digital Earth*, 6(1), 134–156.

- Sun, D., R.T. Pinker, and J.B. Rasara, 2004, Land surface temperature estimation from the next generation of Geostationary Operational Environmental Satellites: GOES M-Q,” *Journal of Applied Meteorology*, 43, 363–372.
- Tang, R., Z.L. Li, and B. Tang, 2010, An application of the Ts-VI triangle method with enhanced edges determination for evapotranspiration estimation from MODIS data in arid and semi-arid regions: Implementation and validation,” *Remote Sensing of Environment*, 114, 540–551.
- Wang, K., Z. Li, and M. Cribb, 2006, “Estimating of evaporative fraction from a combination of day and night land surface temperature and NDVI: A new method to determine the Priestley-Taylor parameter,” *Remote Sensing of Environment*, 102(3–4), 293–305.
- Xu T.R., S. Liang, and S. Liu., 2011, Estimating turbulent fluxes through assimilation of geostationary operational environmental satellites data using ensemble Kalman filter,” *Journal of Geophysical Research*, 116.
- Zhang, Y.C., C.N. Long, W.B. Rossow, and E.G. Dutton, 2010, Exploiting diurnal variations to evaluate the ISCCP-FD flux calculations and radiative-flux-analysis-processed surface observations from BSRN, ARM and SURFRAD,” *Journal of Geophysical Research*, 115.